J. Fluid Mech. (2011), *vol.* 670, *pp.* 240–259.
doi:10.1017/S0022112010005227

Pulsatile jets

RICHARD E. HEWITT AND PETER W. DUCK†
School of Mathematics, The University of Manchester, Oxford Road, Manchester M13 9PL, UK

(Received 22 January 2010; revised 4 October 2010; accepted 4 October 2010;
first published online 12 January 2011)

We consider the evolution of high-Reynolds-number, planar, pulsatile jets in an incompressible viscous fluid. The source of the jet flow comprises a mean-flow component with a superposed temporally periodic pulsation, and we address the spatiotemporal evolution of the resulting system. The analysis is presented for both a free symmetric jet and a wall jet. In both cases, pulsation of the source flow leads to a downstream short-wave linear instability, which triggers a breakdown of the boundary-layer structure in the nonlinear regime. We extend the work of Riley, Sánchez-Sans & Watson (*J. Fluid Mech.*, vol. 638, 2009, p. 161) to show that the linear instability takes the form of a wave that propagates with the underlying jet flow, and may be viewed as a (spatially growing) weakly non-parallel analogue of the (temporally growing) short-wave modes identified by Cowley, Hocking & Tutty (*Phys. Fluids*, vol. 28, 1985, p. 441). The nonlinear evolution of the instability leads to wave steepening, and ultimately a singular breakdown of the jet is obtained at a critical downstream position. We speculate that the form of the breakdown is associated with the formation of a 'pseudo-shock' in the jet, indicating a failure of the (long-length scale) boundary-layer scaling. The numerical results that we present disagree with the recent results of Riley *et al.* (2009) in the case of a free jet, together with other previously published works in this area.

Key words: boundary layer control, boundary layer stability, instability

1. Introduction

We consider the downstream evolution of a pulsatile planar jet in an incompressible, viscous fluid at a high Reynolds number. We investigate the effects of pulsation on two closely related jet flows, namely the symmetric free jet and the wall jet. The free jet solution is often attributed to Bickley (1937) and the wall jet to Glauert (1956); however (as highlighted by a referee to this paper) both solutions can be traced back to Schlichting (1933) (free jet) and Akatnov (1953) (wall jet). In both of these cases, we allow the source of the jet to comprise a mean component with a superposed pulsatile component. The problem is formulated as a two-dimensional, unsteady boundary layer, with one parameter associated with the dimensionless frequency of pulsation, and another which is a measure of the amplitude of pulsation.

This work was motivated by Riley *et al.* (2009, hereafter referred to as RSW), who addressed the same problem in the specific case of the free jet. The analysis of RSW neatly extracted the intricate structure of the linearised perturbation (in the far-downstream region), in the (linear) limit of small pulsation amplitude. It was shown that the linear perturbation consisted of infinitely many spatially decaying modes,

† Email address for correspondence: duck@ma.man.ac.uk

together with a single growing mode. This spatially growing mode was discarded as not being relevant on the basis that numerical solutions of the two-dimensional, nonlinear, boundary-layer equations did not show its presence in the downstream development. However, our contention in this paper is that the mode *is* relevant and should have been observed in the numerical solutions of the nonlinear boundary-layer system. Other related (numerical) works that have failed to reveal the existence of growing eigenmodes include Marzouk *et al.* (2006*a*), which considered the effect of pulsation on a high-Reynolds-number planar jet (with heat transfer effects also included). This work was extended to axisymmetric geometries by them in Marzouk *et al.* (2006*b*).

It is known that the unsteady, two-dimensional classical boundary-layer equations possess a short-wave temporal instability for velocity profiles that contain a local maximum away from a boundary, see Cowley *et al.* (1985). This mode manifests itself as a short-wave viscous instability with unbounded temporal growth rates. It seemed plausible that the Cowley *et al.* (1985) modes of asymptotically short wavelength and high frequency (such that the phase speed of the instability is of the order of the base flow) could have an analogue in periodically forced flows, where one seeks downstream spatial growth. Our claim is that the numerical results of RSW are erroneous, and that a downstream instability *is* found in the form of a propagating wave for both linear and nonlinear pulsation. Therefore, the growing (linear) eigenmode of the RSW analysis cannot be ignored in the nonlinear context. With some extensions, comparable to the work of Cowley *et al.* (1985), we consider a more general jet-like profile and make comparisons with our numerical results. We address the nonlinear evolution of the instability numerically and speculate that a breakdown is achieved at a finite downstream position.

The structure of this paper is as follows. In § 2, we reformulate the problem of pulsatile jets in a general manner that allows consideration of flows of both free-jet and wall-jet types. In § 3, we present the results of the asymptotic analysis of RSW, but reinterpret them in the context of the short-scale instability described by Cowley *et al.* (1985); the analysis is extended to cover both types of jet flows. We present numerical results that show the downstream development of a linear instability that is consistent with the previously discarded eigenmode in the free jet and its analogue in the wall jet. Section 4 presents numerical results in the nonlinear regime, via a spectral decomposition method, and we show clear evidence that the two-dimensional boundary-layer system breaks down at a critical downstream location; some discussion of two comparable (temporal) initial-value approaches is also given (which confirm the conclusions from our spectral computations). In § 5, we make some concluding remarks.

2. Formulation

We begin with the two-dimensional boundary-layer equations for a viscous incompressible fluid of kinematic viscosity ν and formulate the problem in terms of a dimensional streamfunction $\psi^*(x^*, y^*, t^*)$. Here (x^*, y^*) is a Cartesian coordinate system and t^* denotes the dimensional time. We consider an imposed streamwise velocity U, transverse length scale h and a pulsation frequency Ω, such that $\psi^* = Uh\psi$, $y^* = yh$, $x^* = Uh^2x/\nu$ (implying that the Reynolds number $Re = Uh/\nu$, which is of course assumed large) and $t^* = t/\Omega$. This leads to the dimensionless governing equations

$$S\psi_{yt} + \psi_{yx}\psi_y - \psi_{yy}\psi_x - \psi_{yyy} = 0, \tag{2.1a}$$

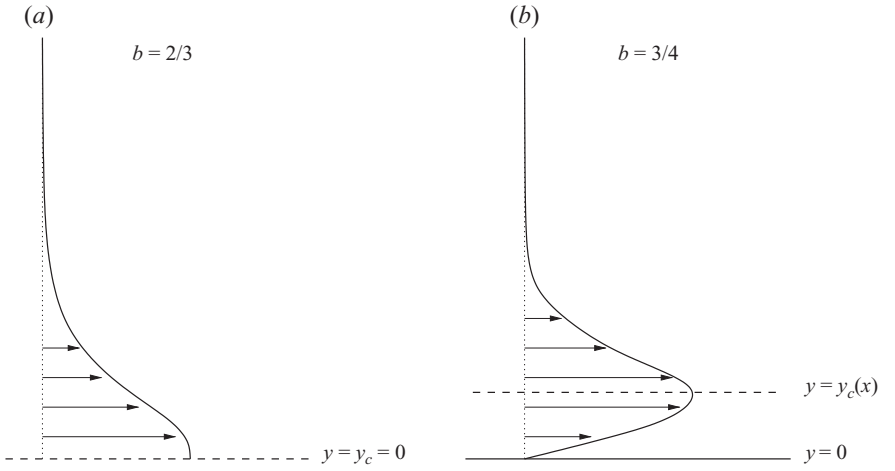

FIGURE 1. Typical streamwise profiles of (a) the steady symmetric free jet and (b) the steady wall jet. As reviewed in § 2.1, the peak streamwise velocity in each case is $U_c(x)$, which decays like $(x+x_o)^{1-2b}$, where $x=-x_o$ is the 'virtual' origin of the jet. The position of this maximum in the boundary layer is such that $y_c \sim x^b$, where $b=3/4$ for the wall jet, and $y_c=0$ for the free jet.

where $S=\Omega h^2/\nu$ and, for a jet flow,

$$\psi_y \to 0 \quad \text{as } y \to \infty. \tag{2.1b}$$

Along the plane $y=0$ we will consider two scenarios, we either impose conditions appropriate for a symmetric free jet,

$$\psi = \psi_{yy} = 0 \quad \text{on } y=0, \tag{2.1c}$$

or no-slip and impermeability conditions appropriate for a wall jet,

$$\psi = \psi_y = 0 \quad \text{on } y=0. \tag{2.1d}$$

To fully specify the problem, we also require the source flow profile

$$\psi = \psi_{source}(y,t) \quad \text{at } x=0, \tag{2.1e}$$

and if considering the (temporal) initial-value problem we would also require the state of the system at $t=0$:

$$\psi = \psi_{init}(x,y) \quad \text{at } t=0. \tag{2.1f}$$

2.1. *Steady base-flow jet profiles*

In the absence of unsteadiness, there are classical similarity solutions for the free jet and wall jet as presented by Bickley (1937) and Glauert (1956), respectively; see figure 1. As discussed by Glauert (1956), one can seek a solution in the form

$$\psi = (x+x_o)^{1-b} G(Y), \tag{2.2a}$$

$$Y = \frac{y}{(x+x_o)^b}, \tag{2.2b}$$

where b is to be determined and $x=-x_o$ is some (in our case 'virtual') origin of the jet. From (2.1a) we observe that the base-flow function $G(Y)$ satisfies

$$G''' + (1-b)GG'' + (2b-1)G'^2 = 0; \tag{2.2c}$$

note that the above equation is invariant under the rescaling

$$G \to CG, \quad Y \to Y/C, \tag{2.2d}$$

for any constant C.

2.1.1. *The free jet: $b = 2/3$*

In the case of a free jet, integrating (2.2*c*) once and applying the boundary conditions $G(0) = G''(0) = G'(\infty) = 0$ is sufficient to show that $b = 2/3$, which is equivalent to the momentum flux being independent of x. Furthermore, the solution can be found analytically, yielding

$$G(Y) = 9^{1/3} \tanh\left(\frac{9^{1/3}}{6} Y\right). \tag{2.3}$$

In this derivation, we have chosen a specific rescaling (2.2*d*) such that the jet has unit momentum flux, and so by making this choice our results are directly comparable to those of RSW.

2.1.2. *The wall jet: $b = 3/4$*

In the case of a wall jet, we integrate (2.2*c*) once, multiply by $G'(Y)$ and integrate again, which on applying the boundary conditions $G(0) = G'(0) = G'(\infty) = 0$ shows that $b = 3/4$ (on the assumption of no reverse flow in the jet). This condition is equivalent to implying that the flux of the exterior momentum flux (arguably, a somewhat unintuitive concept) is independent of x. Although an analytic solution for Y as a function of G can be provided (see Glauert 1956), it is often simpler to solve (2.2*c*) numerically. As with the free jet, we could choose a rescaling (2.2*d*) such that the quantity conserved (the aforementioned flux of the exterior momentum flux) is unity; however, it is more common in this case to simply require that $G(\infty) = 1$. This is equivalent to solving (2.2*c*) as an initial-value problem with the starting data $G(0) = G'(0) = 0$ and $G''(0) = 1/72$.

2.2. *Unsteady pulsatile flow*

Following RSW, we now consider the effects of a pulsatile source on the downstream development of the jet. In particular, we solve the unsteady system (2.1*a*) for $x > 0$ with a source flow at $x = 0$ that takes the form of a self-similar jet profile with $x_o = 1$ and an amplitude $A(t)$. We assume that $A(t)$ consists of a mean-flow component and a superposed periodic pulsation of amplitude ϵ and unit dimensionless frequency. In general, we allow the pulsation-amplitude parameter ϵ to be $O(1)$, and hence

$$\psi_{source}(y, t) = A(t)G(y) = (1 + \epsilon \cos t)\, G(y), \tag{2.4}$$

where G is the appropriate solution for either a wall jet or a free jet. Our observation (in the light of numerous numerical experiments undertaken by the authors) is that the exact nature of the source flow at $x = 0$ does not qualitatively affect the results that we present below.

3. Small-amplitude pulsation: $\epsilon \ll 1$

In the limit of $\epsilon \to 0$, we can seek a solution in the form

$$\psi(x, y, t) = (1 + x)^{1-b} G\left(\frac{y}{(1 + x)^b}\right) + \epsilon \hat{\psi}(x, y, t) + O(\epsilon^2), \tag{3.1a}$$

$$\hat{\psi}(x, y, t) = \tilde{\psi}(x, y)\, \mathrm{e}^{\mathrm{i}t} + \text{c.c.}, \tag{3.1b}$$

where G is the appropriate mean component of the free or wall jet flow, with $b = 2/3$ or $3/4$ respectively (as discussed above), and $\tilde{\psi}$ is the perturbation due to the pulsation. When $\epsilon = 0$, the downstream development of the streamfunction clearly remains self-similar, albeit relative to a virtual origin at $x = -1$. The equations and conditions to be satisfied by the perturbation $\tilde{\psi}$ are simply the linearisation of the full system (2.1).

In the specific case of $b = 2/3$ (a free jet), the work of RSW developed the far-field structure for linear periodic perturbations in the limit $\epsilon \to 0$. For the problem as formulated herein, the RSW analysis shows that the perturbation, in an inner layer adjacent to the axis of symmetry, can be expanded in the form

$$\tilde{\psi} \sim \xi^{k_n} \exp\left(-\frac{\mathrm{i}}{8}\xi + \left(\frac{1}{4} - n\right)\sqrt{\mathrm{i}}\,\xi^{1/2}\right)(f_0(\zeta) + O(\xi^{-1/2})), \tag{3.2a}$$

for $\xi \gg 1$, where $\zeta = \sqrt{\mathrm{i}\xi}G^2$ is an inner variable and

$$\xi = \frac{4S}{9}(9(x+1))^{4/3}. \tag{3.2b}$$

In (3.2a), $n = 0, 1, \ldots$ indicates the mode number and k_n is a constant associated with mode n; clearly, the exponential leads to downstream growth for $n = 0$, but decay for all $n \geqslant 1$.

Crucially, much of the analysis of RSW discards the $n = 0$ mode and only considers the $n = 1$ mode. The claimed irrelevance of the $n = 0$ downstream mode was supported by numerical results of the full system (2.1a), which showed a decay of the perturbation in the downstream flow that agreed with the $n = 1$ mode. Interestingly, RSW did observe the $n = 0$ mode in computational solutions of the linearised problem (p. 167, § 4 of RSW), but ignored these because they were not found in the nonlinear analogue; no mechanism for nonlinear inhibition of the $n = 0$ mode was suggested. As mentioned in the Introduction, the related work of Marzouk *et al.* (2006a,b) also failed to find evidence of this downstream-growing eigenmode in numerical results (albeit in a thermally influenced jet).

Our contention here is that the $n = 0$ mode *is* physically relevant and cannot (in general) be ignored, representing as it does, a growing instability in the downstream evolution of the jet. We therefore believe that the numerical results of RSW (and other previous works in the area) are in error, and that an accurate solution of the system (2.1a) will reveal the $n = 0$ instability in both the linear and nonlinear problems. We also show that the instability is sufficiently generic to have an analogue in the wall-jet system.

Numerical results for the linearised problem, which confirm the downstream development of the $n = 0$ mode, are shown in § 3.2. However, before describing these, we first present a discussion of the downstream modes in a general planar-jet flow and relate the downstream instability to that discussed by Cowley *et al.* (1985).

3.1. *The downstream eigenmodes*

To address the downstream evolution of the perturbation $\tilde{\psi}(x, y)$, it is convenient to make the following substitutions:

$$\tilde{\psi}(x, y) = (x+1)^{1-b} f(X, Y), \tag{3.3a}$$

$$X = (x+1)^{2b}, \tag{3.3b}$$

where Y is defined by (2.2b). The linear perturbation equation is then

$$(1-b)(fG)_{YY} - 2(2-3b)f_Y G' + f_{YYY} - \mathrm{i}XSf_Y + 2bX(G''f_X - G'f_{XY}) = 0, \quad (3.3c)$$

where $f(Y=0) = f_Y(Y \to \infty) = 0$ and either $f_{YY}(Y=0) = 0$ for the free jet ($b = 2/3$) or $f_Y(Y=0) = 0$ for the wall jet ($b = 3/4$). This equation is essentially (after some rescaling) equation (3.8) of RSW; however, here it applies (via b) to both classes of planar jets.

For a general planar jet profile, there is a single point of vanishing shear at $Y = Y_c$, where $G''(Y_c) = 0$; for the free jet, this point is obviously at $Y_c = 0$. In the bulk of the domain with $Y > Y_c$, a leading-order balance far downstream is between the last three terms of (3.3c) for $X \gg 1$. We can seek a periodic travelling-wave solution of the form

$$f(X, Y) = \exp(-\mathrm{i}\bar{\Theta}(X))(f_0(Y) + \cdots), \quad (3.4)$$

where $\bar{\Theta}_X = K + \cdots$ is the wavenumber. It is straightforward to see that, in such a region, a solution exists in the form

$$f_0(Y) \sim G'(Y) - G'(Y_c), \quad (3.5)$$

provided that the wavenumber is

$$K = \frac{S}{2bG'(Y_c)}. \quad (3.6)$$

This is a leading-order outer solution that does not satisfy the required conditions at $Y = 0$ and a viscous critical layer is required around the point $Y = Y_c$. In the case of the wall jet, there is an additional region between $Y = Y_c$ and the wall for which the appropriate leading-order solution is $f_0(Y) = 0$. This outer solution is essentially equation (5a) from the analysis of Cowley *et al.* (1985); we shall return to the contribution of the viscous layer later.

In terms of the unscaled (original) spatial coordinates (x, y), the above solution corresponds to a streamfunction for the perturbation in the form

$$\hat{\psi} \sim \exp(-\mathrm{i}\theta(x, t) + \cdots)(\hat{\psi}_0 + \cdots), \quad (3.7)$$

where the leading-order phase function is

$$\theta(x, t) = \frac{S(x+1)^{2b}}{2bG'(Y_c)} - t. \quad (3.8)$$

Thus, the perturbation (far downstream) is an asymptotically short-scale wave propagating in the downstream direction with a (large) wavenumber of

$$k(x) = \frac{S(x+1)^{2b-1}}{G'(Y_c)}. \quad (3.9)$$

We note that this is in agreement with (3.2) (as obtained for the free jet by RSW) on substitution of $b = 2/3$, $Y_c = 0$ and $G'(Y_c) = 3^{1/3}/2$. The phase speed (c_p) of the instability wave is slow due to the deceleration of the underlying jet flow:

$$c_p(x) = G'(Y_c)(x+1)^{1-2b}S^{-1} = U_c(x)S^{-1}, \quad (3.10)$$

where $(x+1)^{1-2b}G'(Y_c) = U_c(x)$ is simply the maximum streamwise velocity of the wall/free jet base flow at the downstream location x.

Therefore, at leading order, far downstream, the linear perturbation is a neutral short-scale wave that is propagating at the maximum local speed of the underlying jet

flow. To obtain the spatial growth of this wave and to determine the attenuation due to the non-parallelism of the base flow, we have to include the effect of the viscous layer and higher-order terms.

The behaviour described above has been noted before for short-scale waves in (effectively parallel) boundary-layer flows by Cowley *et al.* (1985). They highlighted that the Tollmien–Schlichting-like wave propagates with the peak streamwise velocity, with the (temporal) growth rate determined in a viscous critical layer around the maximum velocity location. In an inner region, the balance is between viscous effects, f_{YYY}, and the higher-order base flow curvature that arises from $XG''(Y)f_X$. This leads to the new region spanned by $\hat{Y}$, where

$$Y = Y_c + X^{-1/4}\hat{Y}. \tag{3.11}$$

In terms of the original variable y, this translates to

$$y = (x+1)^b Y_c + (x+1)^{b/2}\hat{Y}; \tag{3.12}$$

note that for a free jet (as noted earlier) $Y_c = 0$, again in agreement with RSW.

The results of an analysis in the viscous layer are presented in the Appendix, the main conclusion of which is that the higher-order terms lead to a spatial growth of the periodic wave, with a corresponding small correction to the local wavenumber. The asymptotic form of the perturbation streamfunction, including this downstream growth, is

$$\hat{\psi}(x, y, t) \sim \exp(\mathrm{i}\Theta(X, t))(\hat{\psi}_0 + \cdots), \tag{3.13}$$

$$\Theta(X, t) = -\left(\frac{1}{2bG'(Y_c)}SX - t\right) - \mathrm{i}\sqrt{\frac{(2b-1)}{2b^2G'(Y_c)}}\sqrt{\mathrm{i}SX} + O(\log X). \tag{3.14}$$

3.2. *Numerical solution of the linear system*

Numerical solutions in the limit $\epsilon \ll 1$ are obtained by solving the linearised form of (2.1*a*) for the complex quantity $\tilde{\psi}$ as defined in (3.1). The domain for the computation is $x \in [0, x_\infty]$ and $y \in [0, y_\infty]$, for some domain truncation x_∞ and y_∞; as the jet spreads laterally, y_∞ must be increased as x_∞ is increased. The linear problem was rewritten as a system of first-order equations in the standard form as

$$\boldsymbol{M}_{3\times 3}\,\underline{\tilde{\boldsymbol{f}}}_x + \underline{\tilde{\boldsymbol{f}}}_y = \underline{\tilde{\boldsymbol{R}}}, \tag{3.15}$$

where $\underline{\tilde{\boldsymbol{f}}} = (\tilde{\psi}, \tilde{\psi}_y, \tilde{\psi}_{yy})$, and the matrix $\boldsymbol{M}_{3\times 3}$ and the vector $\underline{\tilde{\boldsymbol{R}}}$ both depend upon the base flow G and position x, y.

The form (3.15) is straightforward to solve by a standard Crank–Nicolson scheme, marching in x from the known source flow at $x = 0$. Equation (3.15) is discretised at the mid-nodal points $(x_{j-1} + x_j)/2$ and $(y_{k-1} + y_k)/2$, using second-order finite differencing. This results in a banded matrix problem with six diagonals at each x_j location, which is solved using the complex banded solver from the LAPACK library, before moving to the next downstream position x_{j+1}. The steps taken to validate the numerical solutions presented here are discussed in § 5; all results presented are independent of the properties of the computational mesh.

In figure 2, we show the downstream evolution of the streamfunction at the edge of the boundary layer for increasing x. It is clearly seen that an instability is obtained both for the free jet and the wall jet. The qualitative features of the instability are the same in both cases, with spatial oscillations of decreasing wavelength being observed, together with rapid spatial growth.

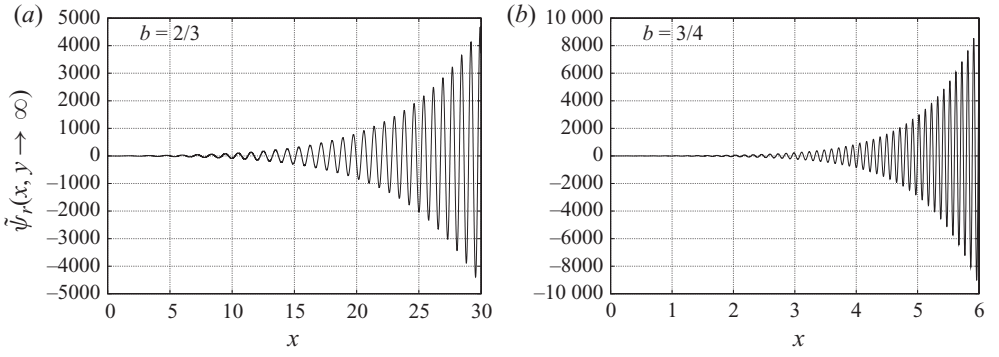

FIGURE 2. The downstream evolution of the real part of the (linear) perturbation streamfunction, $\tilde{\psi}_r(x, y \to \infty)$, at the edge of the boundary layer in the linear limit, with $S = 2$. Shown are (*a*) the free jet and (*b*) the wall jet.

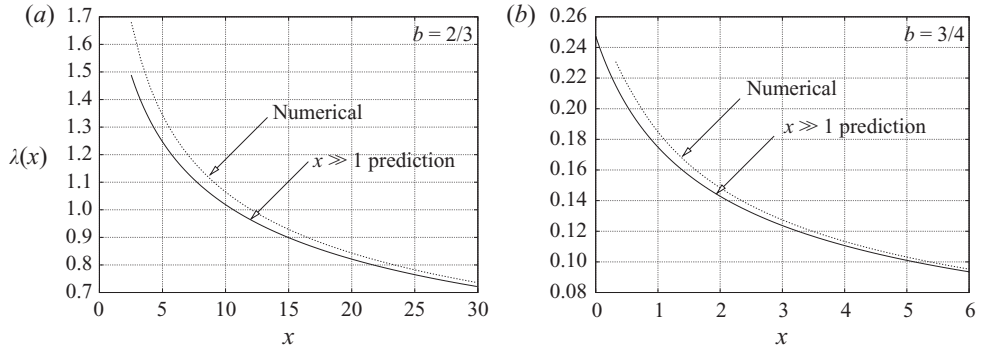

FIGURE 3. The leading-order local wavelength $\lambda(x)$ in the downstream evolution of the linear perturbation for $S = 2$ in (*a*) the free jet and (*b*) the wall jet. In both cases, the solid line is $\lambda(x) = 2\pi/k(x)$, where $k(x)$ is determined from (3.9) whilst the dashed line is obtained from the numerical solution by computation of the locations x_i where $\tilde{\psi}_r(x_i, y \to \infty) = 0$.

In figure 3, we compare the downstream evolution of the local wavelength $\lambda(x) = 2\pi/k(x)$, where $k(x)$ is the local wavenumber, with the asymptotic prediction of (3.9). The local wavelength of the computational solution for $\tilde{\psi}(x, y)$ is taken to be double the separation of two consecutive zeros of $\tilde{\psi}_r(x, y \to \infty)$. The interpretation of the instability as a propagating wave of local wavenumber (3.9) is clearly in agreement with the numerical solution when $x \gg 1$.

In figure 4, we show the downstream evolution of the real part of the perturbation streamfunction evaluated at the boundary-layer edge; $\tilde{\psi}(x, y \to \infty)$. The computational results have been rescaled with the asymptotic prediction for $x \gg 1$ clearly showing a saturated signal, which, as we have already shown in figure 3, has a local wavelength that is also in agreement with the asymptotic description. Similar agreement can be found for other values of S.

The conclusion from the computation of the linearised problem is clearly that the $n = 0$ unstable eigenmode is the dominant response far downstream in both the wall jet and the free jet. We now proceed to the nonlinear problem bearing in mind that the results of RSW showed no instability of the free jet to finite amplitude pulsation of the source flow.

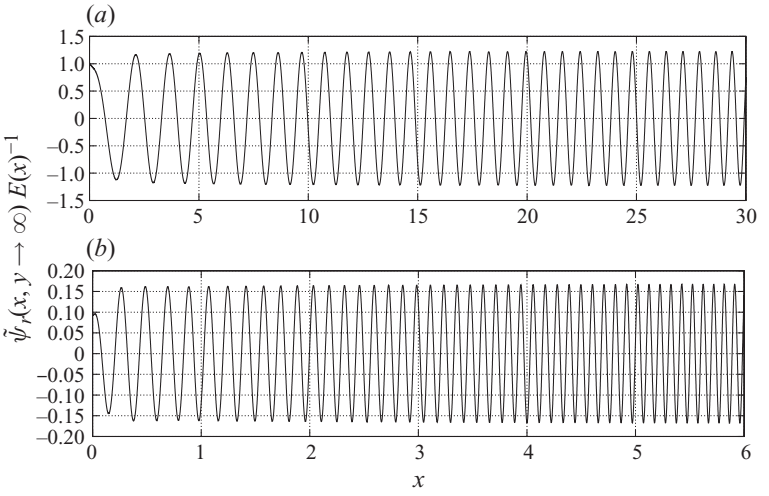

FIGURE 4. The same data as in figure 2, but rescaled by the far-field asymptotic form of the unstable $n = 0$ mode. These results are from parabolic marching of the linear system, with $S = 2$ and (*a*) $b = 2/3$, (*b*) $b = 3/4$. Here, $E(x) = X^{1/4} \exp([(S(2b-1)X)/(4b^2 G'(Y_c))]^{1/2})$ is the asymptotic prediction for the amplitude of the wave perturbation for large X.

4. Nonlinear pulsation: $\epsilon = O(1)$

For the nonlinear pulsatile flow, we may take a spectral decomposition in the form

$$\psi(x, y, t) = \sum_{m=-M}^{m=M} \psi_m(x, y)\, \mathrm{e}^{\mathrm{i}mt}, \tag{4.1}$$

where M is a suitably chosen truncation of the series (typically we chose $M = 50$) and $\psi_{-m} = \psi_m^{(c)}$ (i.e. a change of sign of the index corresponds to complex conjugation). The computational task is to march (parabolically) the fully nonlinear problem (2.1*a*), subject to the following constraint at the source of the jet:

$$\left.\begin{aligned} \psi_0(x = 0, y) = G(y), \quad \psi_1(x = 0, y) = \frac{\epsilon}{2} G(y), \\ \psi_m(x = 0, y) = 0, \ \text{for } m = 2, \ldots, M, \end{aligned}\right\} \tag{4.2}$$

where G is the appropriate free/wall jet solution of (2.2*c*). The boundary conditions at each downstream location are that $\psi_m(y = 0) = \psi_{my}(y \to \infty) = 0$ and either $\psi_{myy}(y = 0) = 0$ for $b = 2/3$ (free jet) or $\psi_{my}(y = 0) = 0$ for $b = 3/4$ (wall jet), where $m = 0, \ldots, M$.

Again, we apply a standard second-order scheme, with mid-point evaluation of the equations on the truncated computational domain $[0, x_\infty] \times [0, y_\infty]$. At each x station, the nonlinear boundary-value problem for $\psi_0, \ldots, \psi_M$ is solved by iteration (with complex conjugation invoked for $m < 0$). The iteration scheme involved computing each value of m in turn (starting with $m = 0$), repeatedly until convergence was achieved. Sparseness was fully exploited in the solution of the algebraic system.

Figures 5(*a*) and 5(*b*) show results for the real and imaginary components (respectively) of $\psi_m(x, y \to \infty)$ in the case of a free jet, with $S = 2$ and $\epsilon = 0.05$, for $m = 0, 1, 2, 3$. Just beyond the final downstream location shown, the computations ceased to converge. This convergence failure was found to be a consistent feature

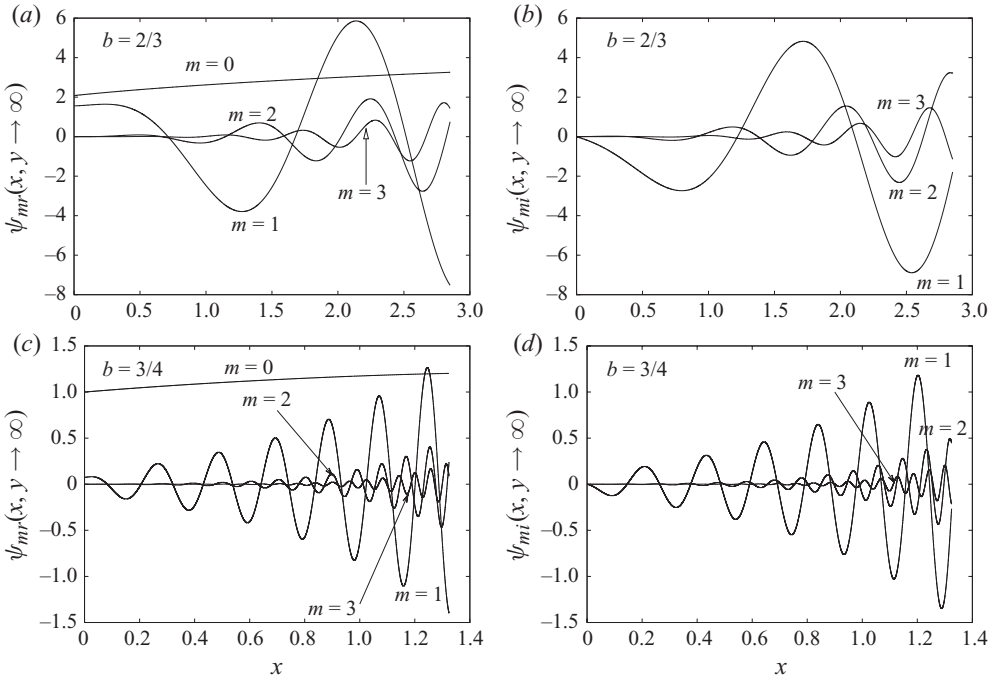

FIGURE 5. The downstream evolution of $\psi_m(x, y \to \infty)$ for $m = 0, 1, 2, 3$ and $S = 2$. The real and imaginary parts are shown in (a) and (b) respectively for the free jet with $\epsilon = 0.05$, whilst (c) and (d) show the real and imaginary parts (respectively) for the wall jet with $\epsilon = 0.005$. Note that, for clarity compared to $m = 0$, the values for $m = 1, 2, 3$ have all been increased by a factor of 30.

in all of our nonlinear spectral computations covering a broad range of values of ϵ and S. The same feature was also observed in the nonlinear wall-jet calculations for $\psi_m(x, y \to \infty)$, as presented in figures 5(c) and 5(d) with $S = 2$ and $\epsilon = 0.005$, for $m = 0, 1, 2, 3$. In both the above sets of results, downstream oscillation and growth is observed in the $m > 0$ modes, although the failure of the numerical scheme occurs considerably earlier in the case of the wall jet (given the same value of ϵ). Based purely on our previous analysis for the downstream growth of linearised perturbations, we should expect a more rapid development in the case of a wall jet, primarily because the peak downstream velocity $G'(Y_c)$ is an order of magnitude smaller in our formulation.

To investigate the failure of the numerical scheme further, let us revisit the (free-jet) case considered in figures 5(a) and 5(b), in particular the higher modes, $m = 10$, 20, 30, 40. Results for the real and imaginary components of $\psi_m(x, y \to \infty)$ are presented in figures 6(a) and 6(b), respectively (note the scalings employed, in order to adequately present these results on the same scale). The rapid oscillation and growth of the higher modes is clearly seen, very much in line with the linearised results described earlier in this paper (higher modes can loosely be regarded as being equivalent to larger values of S). Similar effects were observed in the corresponding wall-jet results.

A close observation of the results described above, and others produced from computation, revealed no singular/unusual behaviour in any of the physical quantities at the point of iterative-convergence failure. However, as a test of the convergence of the Fourier expansion (4.1), figure 7 shows a simple ratio test for the free-jet case. Specifically, we examine the ratio $|\psi_{48}(x, y \to \infty)|/|\psi_{47}(x, y \to \infty)|$; this figure clearly

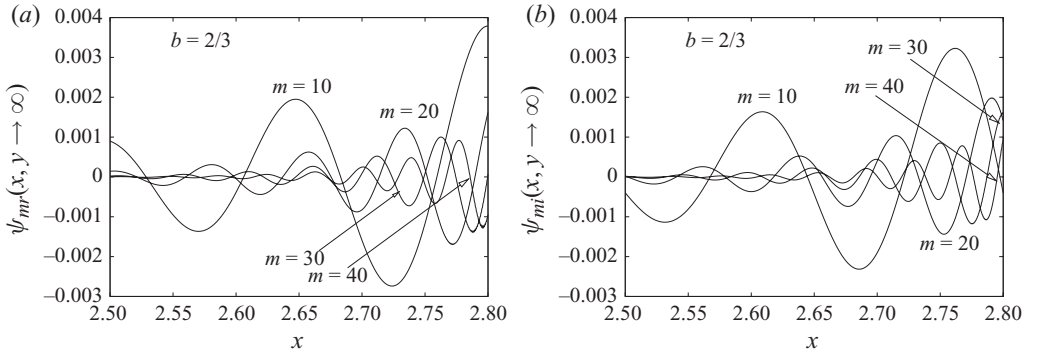

FIGURE 6. The (*a*) real and (*b*) imaginary parts of $\psi_m(x, y \to \infty)$ for the free jet with $m = 10, 20, 30, 40$, $S = 2$ and $\epsilon = 0.05$. Note that values for $m = 20, 30, 40$ have been increased by factors of 10, 100 and 1000, respectively, and that the range of x here is truncated to only $x > 2.5$.

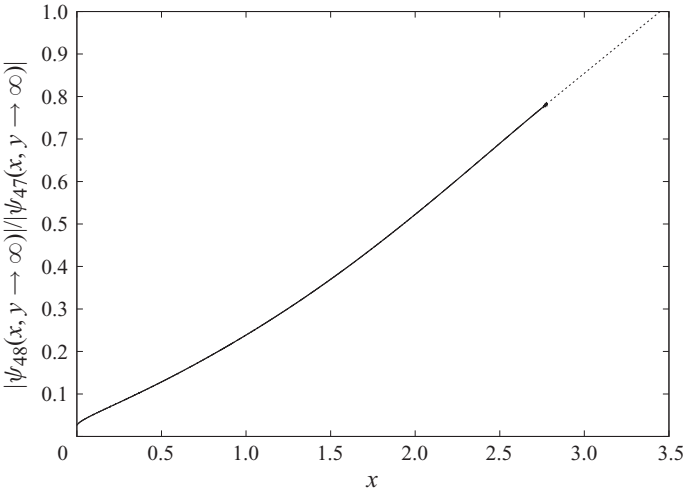

FIGURE 7. The ratio test for $\psi_m(x, y \to \infty)$ using the 47th and 48th modes with $S = 2$, $\epsilon = 0.05$, $b = 2/3$ (a free jet). Note that other choices of mode number and other physical quantities provide consistent results. The dashed line indicates an extrapolation to predict the critical downstream position.

suggests a monotonic growth in this quantity. Other values of m, and other (physical) quantities, were analysed, which led to very similar results as those presented in figure 7. Clearly, a breakdown of the series (4.1) must occur when the ratio test reaches unity. Figure 7 indicates an extrapolated value for which the series fails, which appears to occur approximately at $x = 3.45$.

It is interesting to investigate the effect of varying ϵ on the location of the predicted breakdown of (4.1). Figure 8 shows the critical downstream position, with results obtained by extrapolating the ratio test results (to determine the x-location where the ratio test yields unity) over a range of pulsation amplitudes ϵ, and it is clear that as $\epsilon \to 0$, $x_c \to \infty$, as indeed it must.

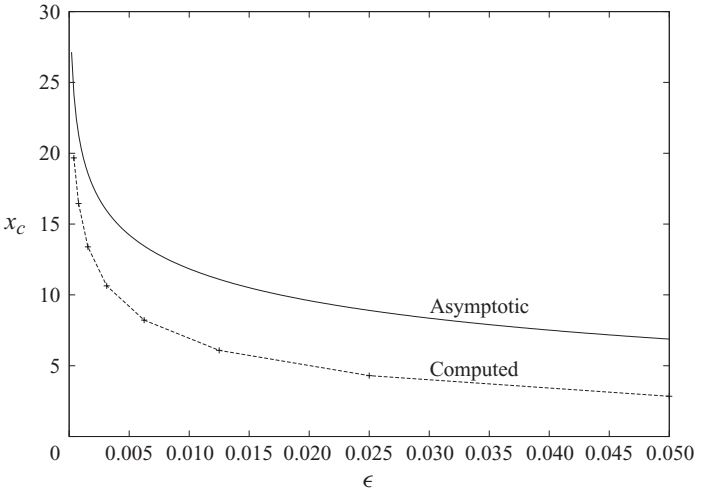

FIGURE 8. The prediction of the critical downstream location of a boundary-layer breakdown, $x_c(\epsilon, S)$, based on the scaling argument of § 4, compared to a numerical extrapolation of the point of non-convergence of the spectral decomposition (4.1). The behaviour of the breakdown point as a function of the pulsation amplitude ϵ is shown in the case of $S = 2$ and $b = 2/3$ (the free jet).

Given that the breakdown is observed at small values of the pulsation amplitude ϵ, it is instructive to consider the development of a solution in the following form:

$$\psi(x, y, t) = (1+x)^{1-b} G\left(\frac{y}{(1+x)^b}\right) + \epsilon\psi_{11}(x, y)\,\mathrm{e}^{\mathrm{i}t} + \epsilon^2(\psi_{20}(x, y) + \psi_{22}(x, y)\,\mathrm{e}^{2\mathrm{i}t}) + \cdots . \tag{4.3}$$

From our previous discussion of the linearised modes, the first harmonic (in the linear limit) is such that

$$\psi_{11}(x, y) \sim \exp(\gamma\sqrt{SX})\bar{\psi}_{11}(x, y), \tag{4.4}$$

where $\bar{\psi}_{11}$ grows at most algebraically in the downstream direction and X is again defined by (3.3*b*). In this expression, the constant $\gamma = ((2b-1)/(4b^2G'(y_c))^{1/2}$ (as determined in the Appendix).

Obviously, the response of the system becomes fully nonlinear, irrespective of the pulsation amplitude, if $\epsilon\psi_{11} = O(1)$. Furthermore, the downstream forced response of the mth harmonic, for example, will be of the form

$$\epsilon^m\psi_{mm}(x, y) \sim \exp(m\gamma\sqrt{SX})\bar{\psi}_{mm}(x, y), \tag{4.5}$$

where $\tilde{\psi}_{mm}$ grows at most algebraically with x. Hence, all terms in (4.3) can become $O(1)$ simultaneously at the critical downstream location, x_c, which is a function of the pulsation amplitude ϵ and S. This breakdown of (4.3) will occur when the ratio

$$\frac{\epsilon^{m+1}\exp((m+1)\gamma\sqrt{SX})}{\epsilon^m\exp(m\gamma\sqrt{SX})} \tag{4.6}$$

is not exponentially small, which suggests a critical location of

$$x_c = \left(-\frac{1}{\gamma\sqrt{S}}\log\epsilon\right)^{1/b} + O(1)\,. \tag{4.7}$$

Although this asymptotic argument might first be regarded as heuristic, we do not believe this to be the case. Given that the linear regime is rather long ($O((-(1/\gamma\sqrt{S})\log\epsilon)^{1/b})$), it is our assertion that as soon as the flow becomes fully nonlinear, the breakdown occurs rather quickly (i.e. on a shorter length scale).

In figure 8, we include the prediction (4.7) for comparison with the numerically predicted breakdown point of the series (4.1). The agreement is encouraging, especially given the preponderance of logarithmic terms, which lead to an $O(1)$ correction to x_c.

4.1. *Initial-value calculations with* $\epsilon = O(1)$

To pursue the nature of the breakdown in the vicinity of $x = x_c$ further, we consider an initial-value computation rather than a spectral decomposition. It is worth emphasising that the results of Cowley *et al.* (1985) are sufficient to show that such an approach should be susceptible to a temporal short-wave instability at high resolution; therefore, some care is required in undertaking these computations.

To shed some light on this apparent breakdown, we used two independent numerical schemes. The first was a slight modification of the method of Ruban & Vonatsos (2008), in which the boundary-layer equations are formulated in conservative form together with (first-order accurate) marching in x and t. The original formulation of Ruban & Vonatsos (2008) also appears to be first order in y; however, we modified this slightly, by discretising the continuity equation at a mid-nodal point, thereby ensuring second-order accuracy in y. The second scheme is a standard Keller box method (see Keller 1978), in which we write the nonlinear system in the form

$$\boldsymbol{M}^{(1)}_{3\times3}\,\underline{\boldsymbol{f}}_t + \boldsymbol{M}^{(2)}_{3\times3}\,\underline{\boldsymbol{f}}_x + \underline{\boldsymbol{f}}_y = \underline{\boldsymbol{R}}\,, \tag{4.8}$$

where $\underline{\boldsymbol{f}} = (\psi, \psi_y, \psi_{yy})$, $\boldsymbol{M}^{(1)}_{3\times3}$ is a constant mass matrix and the matrix $\boldsymbol{M}^{(2)}_{3\times3}$ and the vector $\underline{\boldsymbol{R}}$ depend upon $\underline{\boldsymbol{f}}$. The nonlinear system (4.8) is solved by Newton iteration after discretisation at the mid-nodal points $(t_{i-1}+t_i)/2$, $(x_{j-1}+x_j)/2$ and $(y_{k-1}+y_k)/2$, with second-order-accurate central differencing of all derivatives. At each time level t_i, we sweep through x_j and, for each downstream position, solve a banded matrix problem (with six diagonals, using the double-precision LAPACK banded solver) until (4.8) is satisfied at the mid-nodal point to a tolerance of less than 10^{-8}. Although all the results we present in this section are for the free jet, we have performed similar computations for the wall jet and found the same qualitative behaviour.

The initial condition is taken to be a self-similar jet flow perturbed by just the first harmonic:

$$\psi(x, y, t = 0) = (1 + x)^{1-b} G\left(\frac{y}{(1 + x)^b}\right) + \epsilon\psi_1(x, y), \tag{4.9}$$

with all other boundary conditions as before. Here ψ_1 is determined from the linearised equations, but it is then imposed at finite amplitude as the initial condition in the nonlinear initial-value problem, i.e. $\psi_1(x, y) = \hat{\psi}(x, y, t = 0)$. On marching forward in time, and discarding any initial transients, we can then examine the spatial development of the flow once the solution is periodic in time.

In figure 9, we show a cross-section of the downstream velocity of the free jet, $u(x, y, t) = \psi_y$, as measured at the arbitrary point of $y = 6$. Because we are presenting the off-axis velocity, and the jet is thickening downstream, the value increases with x over the range shown. The profiles are shown at times $t = 0, \pi/2, \pi, 3\pi/2$ during one cycle of the periodic flow.

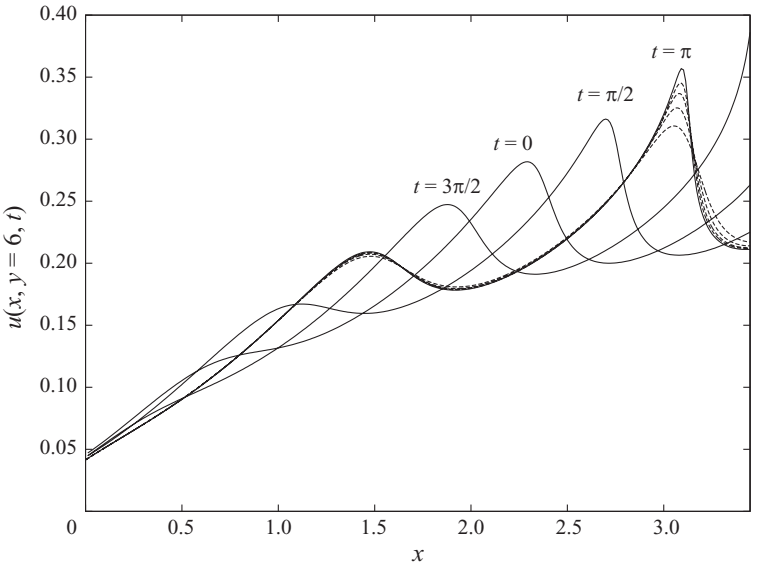

FIGURE 9. The evolution of $u(x, y=6, t)$ over one period of the motion as obtained from a nonlinear initial-value computation for the free jet with $\epsilon = 0.05$, $S = 2$. The results are shown for $x \in [0, x_c]$, where x_c is the point predicted in figure 7 for the failure of the spectral decomposition (3.1). The solid line represents a solution obtained using the second-order Keller box scheme with grid sizes $\Delta x = 1/100$, $\Delta t = \pi/128$, whereas dashed lines show results (at just one time value) of the first-order scheme with spatial/temporal step sizes of $\Delta x = 1/200, \ldots, 1/1600$ and $\Delta t = \pi/256, \ldots, \pi/2048$.

There is some suggestion in the results of figure 9 that the breakdown is associated with wave steepening. The downstream flow velocities remain $O(1)$, but the streamwise gradients of the u-velocity component become increasingly large.

To view this wave steepening in more detail, we examine the perturbation to the streamwise velocity due to the $O(\epsilon)$ pulsation:

$$u_{pert}(x, y, t) = u(x, y, t) - u_{free}(x, y), \tag{4.10}$$

where u_{free} is the well-known steady similarity solution that is achieved in the absence of any pulsation (i.e. when $\epsilon = 0$). In figure 10(a), we show the downstream evolution of u_{pert} for $t = 11\pi/8$, as measured on the axis of symmetry $y = 0$ for the case of $\epsilon = 0.05$ and $S = 2$. The figure also highlights the nodes, at which $u_{pert} = 0$, by the open/filled circular data points. Of key importance to the speed of propagation of these nodes, in the nonlinear regime, is the sign of the quantity

$$\mu = \frac{\partial u_{pert}}{\partial x}. \tag{4.11}$$

In figure 10(b), the open circle denotes the nodes in expansive regions with $\mu > 0$ whilst filled circles denote nodes in compressive regions with $\mu < 0$. In figure 10(b), we track the speed of downstream propagation of these nodal points at the same parameter values of $\epsilon = 0.05$ and $S = 2$. In the linear regime, the nodal points obviously propagate with a speed that is independent of the sign of μ, but the influence of nonlinearity (as shown for $\epsilon = 0.05$) is to decrease the propagation speed where $\mu < 0$ and to increase it where $\mu > 0$. The net effect of nonlinearity is therefore an evolution towards an 'N wave' profile in the perturbation to the streamwise velocity.

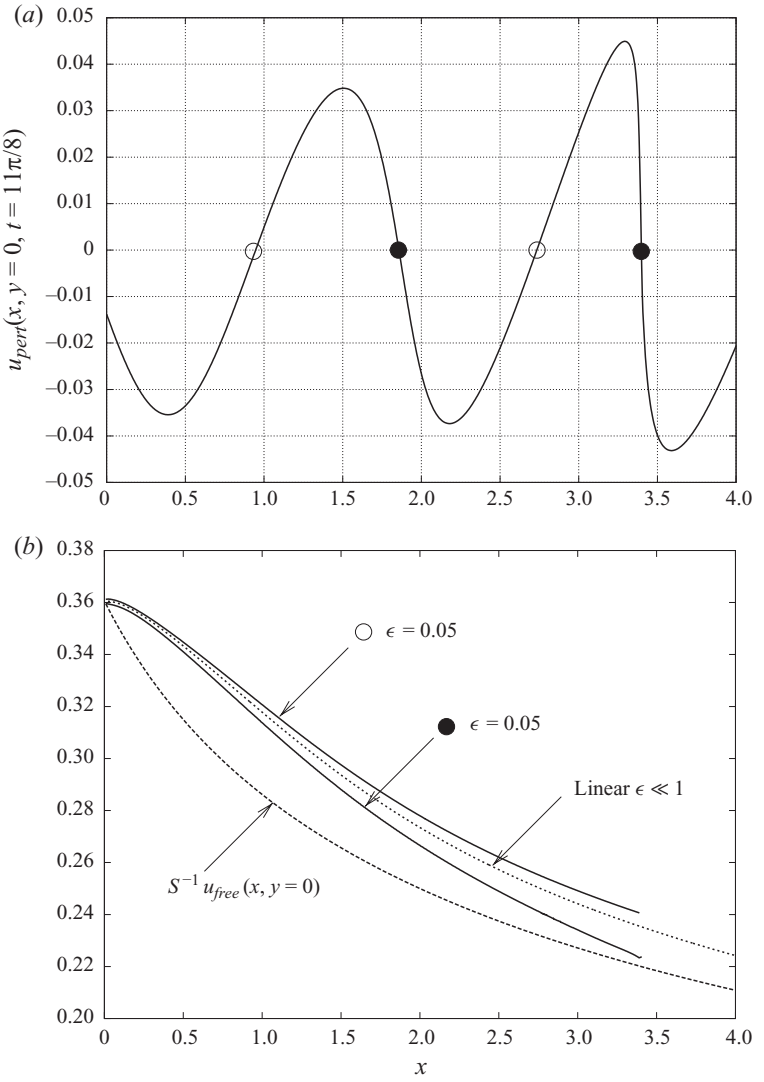

FIGURE 10. (*a*) The perturbation to the streamwise velocity component on the (free) jet axis ($y = 0$) at a time $t = 11\pi/8$. The wave steepening near $x \approx 3.5$ is clearly seen; $\epsilon = 0.05$, $S = 2$, $b = 2/3$. The open/filled circles indicate where $u_{pert} = 0$, with a positive/negative gradient respectively. (*b*) The speeds of propagation of the open/filled circles (as shown in *a*) as a function of downstream distance. Also shown is the linearised prediction for $\epsilon \ll 1$ and the peak downstream velocity of the free jet $u_{free}(x, y = 0)$.

As the wave perturbation propagates downstream, a monotonic increase in u_x is achieved, and our conjecture is that u_x becomes singular at the breakdown position $x = x_c$. In support of this conjecture, figure 11 shows the maximum transpiration of the perturbation at the edge of the boundary layer over one period of the motion. From mass conservation, if $u_x \to \infty$ as $x \to x_c$ then it is also necessary that $v(y \to \infty) \to \infty$ as $x \to x_c$. Figure 11 provides strong evidence to support this conclusion and suggests that the jet boundary layer erupts at $x = x_c$. Note that an estimate of this location, for the case shown in figures 9 and 11, is $x_c \approx 3.45$, consistent with the critical location suggested by figure 7.

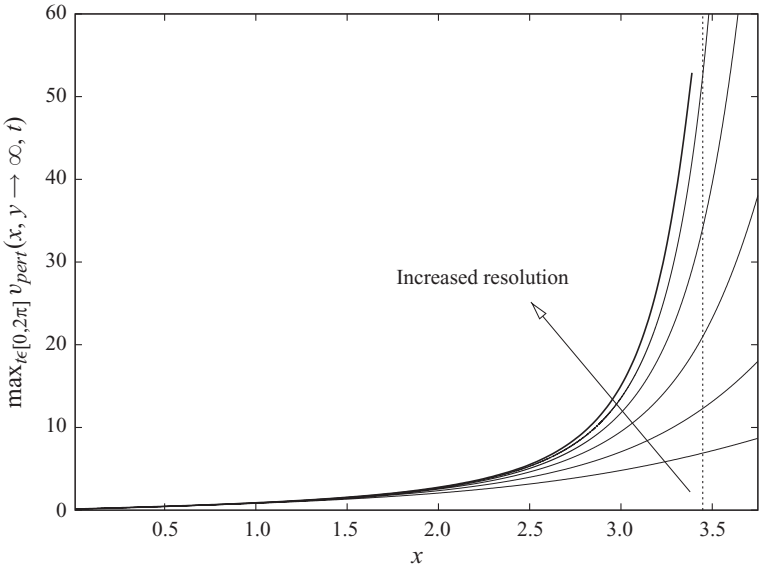

FIGURE 11. The maximum perturbation to the transpiration at the edge of the (free) jet measured over one complete period of the motion, as obtained from a nonlinear initial-value computation with $\epsilon = 0.05$, $S = 2$. The extrapolated breakdown position x_c (as presented in figure 7) is shown at the vertical dashed line. The thick solid line represents a solution obtained using the second-order Keller box scheme with $\Delta x = 1/100$, $\Delta t = \pi/128$, whereas the thin lines show results of the first-order scheme with spatial/temporal step sizes of $\Delta x = 1/200, \ldots, 1/3200$ and $\Delta t = \pi/256, \ldots, \pi/4096$.

5. Discussion

Inspired by the recent analysis of RSW, this paper discusses the spatiotemporal behaviour of pulsatile planar jets. We have extended the far-field analysis of RSW to cover a more general jet flow, considering the wall jet in some detail. The far-downstream linear response corresponds to a short-wave instability that propagates at the maximum speed of the downstream jet flow and the spatial growth is determined in a viscous layer that straddles the point of zero shear in the boundary layer. In this regard, it appears that the wave is a spatially growing analogue of the temporal short-wave instability first described by Cowley *et al.* (1985).

Although our linear asymptotic analysis is in complete agreement with RSW in the specific case of the free jet, our nonlinear numerical results are in stark contrast. Our results indicate that the effect of jet pulsation is to trigger a spatially growing instability that increases rapidly downstream (cf. the linear case). As we disagree on the numerical evolution of the jet, we have taken great care to validate our numerical schemes, and in total we have four separate formulations of related problems, each of which is approached by a different method. We solve the linearised decoupled problem via second-order-accurate parabolic marching, the nonlinear problem is tackled by spectral decomposition, and we have two independent formulations of the initial-value problem. Careful comparisons have shown consistency across all approaches. Furthermore, we have tested convergence of the nonlinear codes to the known self-similar base flow in the case of $\epsilon = 0$ and, although we have not presented the details herein, we have ensured that the numerical data (from all formulations) satisfy the (time-averaged) conservation of downstream momentum flux for the free jet (that is, condition (2.7) as given in RSW).

We note in passing that our condition at $x = 0$ is chosen to be simpler than that tackled by RSW, who chose a smoothed top-hat profile as the source of the jet. However, we did perform similar calculations, and our experience is that changing the nature of the jet at $x = 0$ had no effect on any of the dominant features that we present in this work.

We note that the initial-value problem tackled by RSW should be susceptible to short-wave modes, i.e. refinement of the numerical scheme should produce temporally growing, short-wave, high-frequency perturbations of precisely the sort predicted by Cowley *et al.* (1985). In this regard, we should highlight that the second-order-accurate scheme that we use in § 4.1 does ultimately develop such modes under continued grid refinement in precisely the same manner as discussed by Cowley *et al.* (1985). The convective nature of these unstable modes means that they eventually propagate out of the truncated computational domain, leaving behind a temporally periodic solution.

The short-wave instability present in the numerical initial-value problem is what led us to tackle the evolution of the boundary-layer system via the spectral decomposition (4.1). The numerical spatial marching of this system is well-posed as the system is being forced with a single $O(1)$ frequency/wavenumber perturbation at $x = 0$; hence, the only mechanism to generate the higher harmonics is the nonlinearity of the governing boundary-layer system. Interestingly, the nonlinear cascade to higher modes coupled to the jet deceleration provides a mechanism to convert the $O(1)$ frequency/wavenumber input into a short-wave/high-frequency instability downstream, even for small pulsation amplitudes. The conversion of larger-scale perturbations to a high-frequency/small-wavelength mode in the downstream limit is reminiscent of the papers of Lam & Rott (1993) and Ackerberg & Phillips (1972), in which free-stream oscillations develop into damped short-wave (in the context of boundary-layer flows) modes downstream, which Goldstein (1983) showed then feed into Tollmien–Schlichting waves far downstream. However, in this spatially unstable case, the higher modes grow more rapidly in the downstream direction, which leads to a sudden breakdown of the boundary layer at a point where all modes in the spectral decomposition become of comparable order, leading to streamwise length scale variations comparable to the boundary-layer thickness.

Our conjecture is that the nonlinear breakdown of the pulsatile flow is associated with a steepening of the wave, with an infinite streamwise gradient being obtained at a finite downstream location. Such regions have been labelled 'pseudo-shocks' by Ruban & Vonatsos (2008), who proposed that discontinuous solutions to the boundary-layer equations exist. The behaviour we observe here has many similarities with their results; however, we are not triggering the 'shock-like' transition by an impulsive start, rather it develops naturally from an otherwise smooth flow. Of course these structures are 'pseudo-shocks' in the sense that they only occur over the $O(Re\,h)$ boundary-layer streamwise length scale. They are an indication of a breakdown of the boundary-layer assumption, and a need for a broader set of field equations, notably one that re-includes a transverse variation in pressure. In the analysis of Ruban & Vonatsos (2008), the internal structure of the breakdown region was connected to a square inviscid region of the order of the jet width, and it may prove possible to develop a similar behaviour here.

Our numerical results indicate that, near the first appearance of the breakdown, the acceleration and nonlinear advection terms clearly dominate over viscous diffusion in the bulk of the boundary layer. A further striking feature of our results is that the position at which $|u_x| \to \infty$ appears to be independent of y. As highlighted by

Ruban & Vonatsos (2008) this second point is inevitable as diffusion in y would act to smooth any discontinuity that was not perpendicular to the jet axis. However, this y-independence must constrain the form of the solution in the neighbourhood of any proposed discontinuity and one may wonder if the breakdown is entirely inviscid in nature. Let us suppose that the streamfunction has a single propagating discontinuity at a downstream point $x_s(t) > x_c$ such that

$$\psi = \psi_L(y,t) + (\psi_R(y,t) - \psi_L(y,t))H(x - x_s(t)), \tag{5.1}$$

where H is the Heaviside function and R/L are the values to the right/left of the point $x_s(t)$, respectively. On integrating the streamwise momentum equation (2.1a) from x_s^- to x_s^+ we obtain the constraint

$$S\dot{x}_s(t) = \frac{1}{2}(\psi_R'(y,t) + \psi_L'(y,t)) - \frac{1}{2}\left(\frac{\psi_R''(y,t) + \psi_L''(y,t)}{\psi_R'(y,t) - \psi_L'(y,t)}\right)(\psi_R(y,t) - \psi_L(y,t)), \tag{5.2}$$

where the prime and dot notation indicates differentiation with respect to y and t, respectively. The first term in (5.2) is the usual constraint for the nonlinear advection equation ($u_t + uu_x = 0$), but for an incompressible flow we must retain a contribution from the vu_y term because v has a delta-function-like response, as evidenced from (5.1).

For a free jet, the data in figure 10(a) suggest that, on $y = 0$, if a jump develops in u_{pert} it does so in such a way that $u^R_{pert} + u^L_{pert} \approx 0$. Using this approximation and assuming that (5.2) holds on $y = 0$, leads to $S\dot{x}_s(t) \approx u_{free}(x, y = 0)$, which is consistent with numerical data for the shock speed at the point of formation as shown by the data of figure 10(b).

However, (5.2) should be applied with some caution. In the simpler case of an impulsively started free-jet ejected into an otherwise quiescent flow, as considered by Ruban & Vonatsos (2008), all subscript R terms are zero, and then (5.2) leads to the solution

$$\psi_L = \psi_\infty(1 - A\exp(-2S\dot{x}_s(t)y/\psi_\infty)), \tag{5.3}$$

for arbitrary ψ_∞ and A (if we impose $\psi_L(y = 0) = 0$ then $A = 1$). Clearly, such a solution cannot satisfy the free jet condition of $\psi_L''(y = 0) = 0$ and diffusion in y must play a role in a subregion, so the breakdown cannot be entirely inviscid in nature. In the absence of an asymptotic description of the region around the breakdown zone, we can only speculate that the solution is discontinuous for the boundary-layer equations on the basis of numerical evidence.

We conclude with some comments on the experimental realisability of this breakdown process. The stability of jets has been discussed extensively, see for example Garg (1981) and Sato (1960). Much of the early work was based on an Orr–Sommerfeld analysis, with later extensions to include some non-parallelism via WKB-like methods. The experimental investigation of Sato (1960) employed a loudspeaker to generate high-frequency disturbances and suggested that the Orr–Sommerfeld approach is in agreement with growing small amplitude waves at a sufficiently high Reynolds number. It was noted that these waves 'develop into turbulence without being accompanied by abrupt bursts or turbulent spots'. We note that it is common to consider turbulent jets in a comparable manner to the laminar case, see for example Glauert (1956), in which case the simple mechanism described herein may be robust enough to still occur.

The breakdown process that we present here for pulsatile jets would be a dramatic event, perhaps linked to roll up of the jet, as was suggested for the impulsively started flow by Ruban & Vonatsos (2008). It may be possible that this breakdown can be observed (in either a DNS calculation or experiment) at finite, large Reynolds numbers, in the absence of perturbations of short wavelength that would otherwise trigger inviscid modes. However, the breakdown in our work is strongly linked to the excitation of a single frequency in the source flow and its subsequent nonlinear development. A more practical view of the significance of our paper is as a mechanism that ultimately feeds into the short wave Rayleigh modes, leading to a critical downstream location where significant high-frequency/short-wavelength perturbations must be present, even for controlled conditions upstream.

Appendix. The viscous layer near $Y = Y_c$

At leading order, we have a perturbation of the underlying jet flow that is periodic in time, and is a propagating wave with local wavenumber given by (3.9). The spatial development of the wave as it propagates downstream is determined from (3.3) in a viscous layer about the location of the maximum streamwise velocity of the jet, defined to be at $Y = Y_c$.

We anticipate that a new asymptotic region will be defined (about $Y = Y_c$) by a balance of the curvature of the streamwise velocity profile, i.e. $G'''(Y_c)$, and the influence of viscous diffusion. In this layer the base flow is

$$G(Y) = G(Y_c) + (Y - Y_c)G'(Y_c) + \frac{(Y - Y_c)^3}{3!}G'''(Y_c) + \cdots, \tag{A 1}$$

and the required balance is

$$f_{YYY} \sim XG''(Y)f_X \sim X(Y - Y_c)G'''(Y_c)f_X, \tag{A 2}$$

which shows that the layer is spanned by the coordinate $\hat{Y}$, where

$$Y = Y_c + X^{-1/4}\hat{Y}. \tag{A 3}$$

Following the work of RSW for the free jet, we seek a solution in the form

$$f(Y) = \hat{f}(\hat{Y}) = \exp(\mathrm{i}a_1 X + a_2 X^{1/2} + \cdots)(\hat{f}_0(\hat{Y}) + \hat{f}_1(\hat{Y})X^{-1/2} + \cdots). \tag{A 4}$$

The leading-order solution is the local wave solution (3.7), for which

$$a_1 = -\frac{S}{2bG'(Y_c)}, \tag{A 5}$$

as presented previously, whilst at next order we obtain

$$\hat{f}_{0\hat{Y}\hat{Y}\hat{Y}} + C\hat{Y}\hat{f}_0 - \left(\frac{C}{2}\hat{Y}^2 - \lambda\right)\hat{f}_{0\hat{Y}} = 0, \tag{A 6}$$

where $C = \mathrm{i}2bG'''(Y_c)a_1$ and $\lambda = -bG'(Y_c)a_2$ is the eigenvalue to be determined.

We note that (A 6) is, in essence, equation (7*a*) in Cowley *et al.* (1985), and they construct a solution in their case. In the present case, we note that (A 6) can be reduced to a standard form by transforming to a rescaled coordinate $z = \hat{Y}^2$, differentiating with respect to z, then rescaling again via $z = \sqrt{2/C}\,\hat{z}$, which leads to

$$g''(\hat{z}) + g(\hat{z})\left(-\frac{5}{16} + \frac{1}{4}\sqrt{\frac{2}{C}}\lambda\hat{z} - \frac{\hat{z}^2}{4}\right) = 0, \tag{A 7}$$

where $g(\hat{z}) = z^{5/4} f_{0zz}(z)$, and $f_0(z) = \hat{f}_0(\hat{Y})$. Equation (A 7) is Whittaker's equation, with solutions $W_{K,3/4}$ and $M_{K,3/4}$, where $K = \lambda/\sqrt{8C}$. As discussed by RSW, symmetry of the solution local to $\hat{Y} = 0$ requires that $K = (1/4) - n$, so the leading eigenmode is $n = 0$, which provides

$$a_2 = \sqrt{\mathrm{i}} \sqrt{\frac{(2b-1)S}{2b^2 G'(Y_c)}}. \tag{A 8}$$

This value of a_2 determines the spatial downstream growth of the wave, which is $\exp(a_{2r}\sqrt{X})$, where $a_2 = a_{2r} + \mathrm{i}a_{2i}$. In obtaining (A 8) we have used (2.2*c*) to rewrite the base flow curvature solely in terms of the maximum streamwise velocity of the jet. Finally we note that on setting $b = 2/3$ and $Y_c = 0$, which is a free jet for which $G'(Y_c) = 3^{1/3}/2$, we recover the downstream growth predicted by (3.2).

In (A 4), if we continue to higher order, then the appearance of logarithmic terms leads to an algebraic attenuation of the downstream growth. We do not present the details here, and refer the interested reader to the more detailed discussion of RSW.

REFERENCES

Ackerberg, R. C. & Phillips, J. H. 1972 The unsteady laminar boundary layer on a semi-infinite plate due to small fluctuations in the magnitude of the free-stream velocity. *J. Fluid Mech.* **51**, 137–157.

Akatnov, N. I. 1953 Propagation of planar laminar fluid jet along rigid wall. *Proc. LPI* **5**, 24–31.

Bickley, W. G. 1937 The plane jet. *Phil. Mag.* **23**, 727–731.

Cowley, S. J., Hocking, L. M. & Tutty O. R. 1985 The stability of solutions of the classical unsteady boundary-layer equation. *Phys. Fluids* **28**, 441–443.

Garg, V. K. 1981 Spatial stability of the non-parallel Bickley jet. *J. Fluid Mech.* **102**, 127–140.

Glauert, M. B. 1956 The wall jet. *J. Fluid Mech.* **1**, 625–643.

Goldstein, M. E. 1983 The evolution of Tollmien–Schlichting waves near a leading edge. *J. Fluid Mech.* **127**, 59–81.

Keller, H. B. 1978 Numerical methods in boundary-layer theory. *Annu. Rev. Fluid Mech.* **10**, 417–433.

Lam, S. H. & Rott, N. 1993 Eigenfunctions of linearized unsteady boundary layer equations. *J. Fluid Engng* **115**, 597–602.

Marzouk, S., Mhiri, H., El Golli, S., Le Palec, G. & Bournot, P. 2006*a* Numerical study of momentum and heat transfer in a pulsed plane laminar jet. *Intl J. Heat Mass Transfer* **46**, 4319–4334.

Marzouk, S., Mhiri, H., El Golli, S., Le Palec, G. & Bournot, P. 2006*b* Numerical study of a heated pulsed axisymmetric jet in laminar mode. *Numer. Heat Transfer* A *Appl.* **43**, 409–429.

Riley, N., Sánchez-Sans, M. & Watson, E. J. 2009 A planar pulsating jet. *J. Fluid Mech.* **638**, 161–172.

Ruban, A. I. & Vonatsos, K. N. 2008 Discontinuous solutions of the boundary-layer equations. *J. Fluid Mech.* **614**, 407–424.

Sato, H. 1960 The stability and transition of a two-dimensional jet. *J. Fluid Mech* **7**, 53–81.

Schlichting, H. 1933 Laminare Strahlausbreitung. *Z. Angew Math. Mech.* **13**, 260–263.